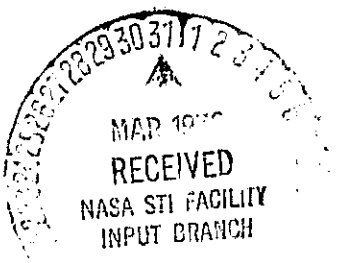

Initialization Procedures for Primitive Equation Models

William K-F. Grant[1] and Eugenia Kálnay de Rivas

Department of Meteorology
Massachusetts Institute of Technology
Cambridge, Mass. 02139

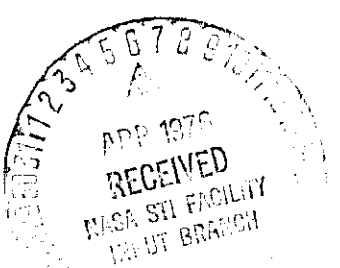

[1] Present affiliation: U.S. Air Force H.Q. Air Weather Service, Scott Air Force Base, Illinois, 62225

Abstract

A linear analysis and comparison of the damping properties of six dynamic initialization schemes is presented, indicating that the Okamura-Rivas scheme has the most efficient damping properties over the whole frequency range, and suggesting that it should be faster than the other methods and give more stable results. The results obtained with a nonlinear shallow water equations model agree well with the linear analysis. The Okamura-Rivas scheme attains complete balance in the equivalent of 5 to 6 hours of leapfrog forecasting, and requires in this model an order of magnitude less computation than the balance equation solution.

1. Introduction

It is well known that the use of observed data directly as initial fields for numerical primitive equation models results in predicted gravity-inertia oscillations with amplitudes far in excess of those observed in the atmosphere. These oscillations may mask the meteorologically significant motions, as was first observed in Richardson's (1922) experiment. The problem is that the observed fields contain excessive imbalances between Coriolis and pressure forces, which arise primarily from observational errors.

Two techniques have been widely used to solve the initialization problem, i.e., to reduce the excessive imbalances between the mass and wind fields.

The first is the balance equation approach, in which the initial mass and wind fields are forced to satisfy some form of the balance equation, from a simple geostrophic approximation to the full nonlinear balance equation. Phillips (1960) suggested that a consistent estimate of the divergent wind should also be obtained from the quasi-geostrophic omega-equation and added to the nondivergent wind determined through the balance equation. Houghton and Washington (1969) and Houghton, Baumhefner and Kasahara (1971) show how this method can be applied on a global scale.

This method is generally satisfactory, but it has disadvantages, some of which are: a) It requires the numerical solution of a set of "diagnostic" type of equations which may not be directly compatible with the prediction equations; b) In extratropical regions, where winds are usually obtained in terms of the mass field, the nonlinear balance equation is of a mixed hyperbolic-elliptic type, and is readily soluble only when purely elliptic. Non-ellipticity occurs in strongly anticyclonic regions where the total vorticity is smaller than one half of the Coriolis parameter. This problem, which as we will see becomes more critical the better the resolution of the model, is usually "solved" by artificially modifying the observed mass fields in non-elliptical regions, but obviously this is not a satisfactory procedure.

The second technique which is becoming increasingly popular is known as "dynamic initialization". In this technique the primitive equations themselves are used to march forward one or several time steps and then return to the initial time by reversing the time step. A damping scheme, as for example Euler- backwards, is used, and if the procedure is repeated, the high-frequency inertia-gravity waves generated by the initial imbalance are eventually damped out (Nitta and Hovermale, 1969). Nitta and Hovermale suggested that the original mass field be recovered after each forward-backward iteration under the assumption that, at least in extratropical regions, measurements of pressure and height fields are more reliable than winds. Partial recovery of the height fields has been proposed by Mesinger (1972) and Winninghoff (1973).

The advantages of the dynamic initialization techniques are two: a) they are very simple to use. The forecast equations (minus the dissipative terms) are used, and therefore the initialized fields are compatible with the forecasting scheme. b) there is no ellipticity constraint when winds are obtained from the mass field. On the other hand, they have a serious disadvantage which is their relative inefficiency. The original Nitta-Hovermale scheme may require several hundred iterations before convergence, equivalent to the number of computations necessary to make a few days' forecast.

A similar, but somewhat more efficient scheme, has been proposed by Mesinger (1972). Temperton (1973) has proposed an initialization scheme in which the fields obtained after forecasting 6 timesteps, say, starting from the initial time, and those obtained by "hindcasting" 6 time-steps starting again from the initial time, are averaged, and the procedure is then repeated. The method is based not on the damping properties of the time scheme, but on the assumption that while large scale meteorologically significant components of the fields will remain largely unchanged, gravity waves generated by the imbalances will be averaged out.

Okamura (see Nitta, 1969, appendix) has proposed a scheme of the Nitta-

Hovermale type, which is simpler and more efficient, but has not found wide use. Kálnay de Rivas has developed a more flexible version of Okamura's scheme which enhances its effectivity, increases its stability and still retains its simplicity.

The purpose of this paper is to compare the balance equation method and the different dynamic initialization techniques. Section 2 contains a brief discussion of the solution of the balance equation. In section 3 we discuss the mathematical properties of the different dynamic initialization methods. The design of the numerical experiments is presented in section 4 and section 5 contains the numerical results.

2. The balance equation approach

The balance equation, as proposed by Charney (1955), is obtained from the divergence equation by neglecting divergence and vertical motion terms, and by assuming a non-divergent wind, $\underset{\sim}{v} = \underset{\sim}{k} \times \nabla\psi$. This yields

$$\nabla^2\phi - f\nabla^2\psi - \nabla\psi\cdot\nabla f + 2\psi_{xy}^2 - 2\psi_{xx}\psi_{yy} = 0. \qquad (2.1)$$

This equation has a maximum relative error O(RiRo), where Ri and Ro are the Richardson and Rossby numbers, and therefore is accurate at least up to 10% even in equatorial regions.

If the stream function ψ is considered known from the observed wind field, the balance equation can be solved to obtain the geopotential ϕ, and is obviously elliptic. On the other hand, if ϕ is taken directly from the data, and (2.1) is solved for ψ, it is easy to show that (2.1) is elliptic if

$$\frac{\nabla^2\phi}{f} - \frac{\nabla f \cdot \nabla\psi}{f} > -\frac{f}{2}. \qquad (2.2)$$

It should be emphasized that this restriction is non-physical, and does not arise when the complete consistent system of balance equations is considered (Charney, 1973). Houghton and Washington (1973) have shown that the solution of (2.1) for ϕ yields more accurate results in the tropics, while the solution for ψ is preferred for extratropical regions. Thus the ellipticity condition may be violated in isolated regions over a substantial portion of the globe.

In extratropical regions the balance equation is usually solved by rewriting eq. (2.1) after Petterssen (1953) and Bolin (1955) as follows:

$$\nabla^2\psi = -f \pm (2\nabla^2\phi + f^2 + A^2 + B^2 - 2\nabla f \cdot \nabla\psi)^{\frac{1}{2}} \qquad (2.3)$$

where $A = \psi_{xx} - \psi_{yy}$ and $B = 2\psi_{xy}$ are the deformation terms. The positive or negative sign of the radical is applicable in the northern or southern hemisphere

respectively. A procedure for solving eq. (2.3) for ψ, called the cycle-scan method by Miyakoda (1956, 1960) and Schuman (1957) consists of evaluating the right hand from a given guess for ψ, and correcting ψ by inverting the laplacian on the left hand side. The pro e usually converges if the ellipticity constraint is satisfied, which also ensures that the right side of 2.3 is real.

3. Analysis of the dynamic initialization methods

In this section we make a linear analysis and comparison of the properties of six dynamic initialization methods. For simplicity, let us represent a set of primitive equations by

$$\frac{\partial u}{\partial t} = \mathcal{F} u \tag{3.1}$$

where u is a column vector of the dependent variables and $\mathcal{F}$ is a matrix differential operator which contains no explicit time derivatives. This equation can be converted into its finite difference (or spectral) equivalent. For example, an Euler marching scheme may be represented as

$$U^{(\tau+1)} = U^{(\tau)} + \Delta t F U^{(\tau)} = (I + \Delta t F) U^{(\tau)} \tag{3.2}$$

where $U^{(\tau)}$ are now discrete values of the dependent variables at time $t = \tau \Delta t$ and F is the finite difference (or spectral) equivalent of $\mathcal{F}$.

The first two schemes we will discuss were suggested by Nitta and Hovermale (1969). The first method, which we will call Nitta-Hovermale 1 or NH1, is the following:

$$U^{*} = U^{(\nu)} + \Delta t F U^{(\nu)} \tag{3.3a}$$

$$U^{(\mu)} = U^{(\nu)} + \Delta t F U^{*}$$

$$U^{**} = U^{(\mu)} - \Delta t F U^{(\mu)} \tag{3.3b}$$

$$U^{(\nu+1)} = U^{(\mu)} - \Delta t F U^{**}.$$

Note that it consists of a single forward time step using the Euler backward or Matsuno scheme (3.3a) followed by a backward time step using the same scheme (3.3b). The superindex (ν) indicates number of iterations, not time, since at the end of a complete iteration we are at the same initial time level.

A recursion relation involving succesive values of $U^{(\nu)}$ is obtained from (3.3):

$$U^{(\nu+1)} = (I + \Delta t^2 F^2 + \Delta t^4 F^4) U^{(\nu)} \tag{3.4}$$

The second method (Nitta-Hovermale 2 or NH2) uses a modified Euler-backward scheme:

$$\begin{aligned} U^* &= U^{(\nu)} + \frac{\Delta t}{2} FU^{(\nu)} \\ U^{**} &= U^{(\nu)} + \Delta t FU^* \\ U^{(\mu)} &= U^{(\nu)} + \Delta t FU^{**} \end{aligned} \tag{3.5a}$$

$$\begin{aligned} \bar{U} &= U^{(\mu)} - \frac{\Delta t}{2} FU^{(\mu)} \\ \bar{\bar{U}} &= U^{(\mu)} - \Delta t F\bar{U} \\ U^{(\nu+1)} &= U^{(\mu)} - \Delta t F\bar{\bar{U}}. \end{aligned} \tag{3.5b}$$

The recursion relation for succesive iterations is

$$U^{(\nu+1)} = (I + \Delta t^2 F^2 - \frac{\Delta t^6}{4} F^6)\, U^{(\nu)}. \tag{3.6}$$

A third method was proposed by Okamura (see Nitta, 1969, Appendix). It involves an explicit Euler time scheme applied forward and backward,

$$U^* = U^{(\nu)} + \Delta t FU^{(\nu)} \tag{3.7a}$$

$$U^{**} = U^* - \Delta t FU^* \tag{3.7b}$$

followed by a linear combination of $U^{(\nu)}$ and U^{**}:

$$U^{(\nu+1)} = 3U^{(\nu)} - 2U^{**}. \tag{3.7c}$$

A fourth method is a generalization of Okamura's method by Kálnay de Rivas, in which (3.7c) is replaced by

$$U^{(\nu+1)} = (n + 1)\, U^{(\nu)} - nU^{**} \tag{3.7d}$$

and n is allowed to vary with ν. It reduces to Okamura's scheme if n = 2. The recursion relation for the Okamura-Rivas (O-R) scheme is

$$U^{(\nu+1)} = (I + n\Delta t^2 F^2)\, U^{(\nu)}. \tag{3.8}$$

Before introducing the last two methods, let us examine the stability and damping characteristics of these four schemes. For this purpose, consider a single harmonic wave of frequency ω in time, $U = U\, e^{i\omega t}$. ω represents any of the characteristic frequencies of the problem (Rossby waves, inertia-gravity waves, etc.), or, more precisely, the eigenvalues of the linearized version of the operator F, and U are the corresponding eigenvectors. Then, the time differencing can be expressed explicitly:

$$\Delta t F U = i\omega \Delta t U = ipU. \tag{3.9}$$

Introducing (3.9) into (3.4), (3.6) and (3.8), we obtain for each method

$$U^{(\nu+1)} = RU^{(\nu)} \tag{3.10}$$

where R is the damping factor corresponding to one <u>complete</u> iteration and is given by

$$\begin{aligned} R &= 1 - p^2 + p^4 && \text{NH1} \\ R &= 1 - p^2 + \tfrac{1}{4}p^6 && \text{NH2} \\ R &= 1 - 2p^2 && \text{O} \\ R &= 1 - np^2 && \text{O-R.} \end{aligned} \tag{3.11}$$

Stability of the iterative methods requires $|R| \leq 1$ and this places a restriction on the size of the time increment Δt:

$$\begin{aligned} \Delta t^2 &\leq 1/\omega_m^2 && \text{NH1} \\ \Delta t^2 &\leq 2/\omega_m^2 && \text{NH2} \\ \Delta t^2 &\leq 2/(n\omega_m^2) && \text{O-R.} \end{aligned} \tag{3.12}$$

Here ω_m is the maximum frequency present in the problem (for example the frequency of the shortest Lamb wave in a primitive equations model). We have assumed in (3.12) that n is fixed, and in that case it is clear that Okamura's

choice of n = 2 maximizes the efficiency of the method.

Fig. 1 shows the absolute value of the damping factors $|R|$ as functions of p for one complete iteration, as in (3.11). The damping of one O-R iteration is shown for n = 1, 2 and 4. Note that NH1 and O-R for n = 2 (Okamura's scheme) show the undesirable property that the highest frequencies ($p \sim 1$) are not damped, and O-R for n = 4 is obviously unstable, even though it is strongly damping for low and mid-range frequencies.

In the O-R method, this can be corrected by allowing n to repeatedly take on a sequence of values during the iterative process. The total damping factor of a sequence is the product of the damping factors at each n of the sequence. The sequence can be chosen in such a way as to maximize the damping both at mid-range and high frequencies. A good example of such a sequence, although not necessarily an optimum one, is n = 1, 1.6, 4. The numbers in this sequence were specifically chosen to correct for the sharp rises in the single-n curves shown in Fig. 1.

It should be noted that the number of computations involved in a single complete iteration depends on the method used. The most costly part of the scheme is the computation of each operation F on U. A meaningful comparison of the cost in computer time required by the methods is therefore the number of F computations required per complete iteration. Another factor that may determine the advantage of a method is the amount of computer memory required, given approximately by the number of sets of the dependent variable U which must be stored separately. Table 1 compares the four methods, as well as Mesinger's and Temperton's methods, on the basis of these practical considerations.

Fig. 2 shows the damping of the NH1, NH2, Okamura and Okamura-Rivas with n = 1, 1.6, 4, after 12 F computations, and therefore compares the relative efficiency of the methods. Note that the O and O-R methods are far more efficient than the NH1 and NH2 methods for low and mid-range frequencies, but only the O-R

Method	# of F per complete iteration	#U stored
NH1	4	2
NH2	6	3
Okamura	2	3
Okamura-Rivas	2	3
Mesinger	4	2
Temperton (N)	2N	3

Table 1: Comparison of number of computations and storage requirements of the iterative schemes.

method exhibits strong damping of high frequencies.

Mesinger (1972) has proposed a marching scheme which is a generalization of the Matsuno and Heun schemes:

$$\begin{aligned} U^{*} &= U^{(\tau)} + a\Delta t F U^{(\tau)} \\ U^{(\tau+1)} &= U^{(\tau)} + \Delta t F U^{*}. \end{aligned} \tag{3.13}$$

The extrapolation factor $\underline{a} = 1$ corresponds to the Matsuno scheme, and $\underline{a} = \frac{1}{2}$ coincides with the Heun scheme. Mesinger suggests the use of this scheme in a forward-backward fashion for dynamic initialization. After a complete iteration, the damping factor is

$$R = 1 - (2a - 1)p^2 + p^4. \tag{3.14}$$

The time step Δt is chosen by Mesinger as $\Delta t = (2a - 1)/(2a^2\omega_m^2)$ so that damping increases monotonically with frequency. Replacing Δt^2 in (3.14) we obtain

$$R = 1 - 2(1 - \tfrac{1}{2}a)\left(\frac{\omega}{\omega_m}\right)^2 + (1 - \tfrac{1}{2}a)^2\left(\frac{\omega}{\omega_m}\right)^4 . \tag{3.15}$$

Then maximum damping is obtained by letting $\underline{a} \to \infty$:

$$R_{MES} = 1 - 2\left(\frac{\omega}{\omega_m}\right)^2 + \left(\frac{\omega}{\omega_m}\right)^4 . \tag{3.16}$$

Note that this method, like NH1 requires 4 F computations to complete one iteration.

A distinct advantage of Mesinger's scheme is that it can also be used as a regular forecasting scheme, in the same way as Matsuno's scheme. However, in order to provide significantly more damping than Matsuno's scheme, $\underline{a}$ has to be much larger than one. The time truncation error of this scheme is

$$\tau = (\tfrac{1}{2} - a)\Delta t \frac{\partial^2 u}{\partial t^2} + \frac{\Delta t^2}{6}\frac{\partial^3 u}{\partial t^3} + \ldots , \tag{3.17}$$

i.e., first order in Δt (unless $\underline{a} = \frac{1}{2}$) and proportional to $\underline{a}$. Mesinger suggests the use of $\underline{a}\Delta t = 6$ hours, but we think this will introduce intolerably large

errors even for synoptic waves.

Fig. 3 compares the damping of the Mesinger and Okamura-Rivas schemes after 12 computations of F. In the O-R scheme, $\Delta t = 1/\omega_m$, so that $p = \omega \Delta t = \frac{\omega}{\omega_m}$. Even though Mesinger's scheme is better than the NH1 and NH2 methods, it is considerably less efficient than the O-R scheme with n = 1, 1.6, 4.

The last scheme that we will discuss is the one proposed by Temperton (1973). He suggests that a forward Euler time step followed by centered leap frog steps be applied so as to obtain $U^{(N\Delta t)}$. Then, starting again from the initial time a similar forecast with negative time step should be executed, obtaining $U^{(-N\Delta t)}$. An iteration is completed by averaging the two forecasts:

$$U^{(\nu+1)} = \tfrac{1}{2}[U^{(N\Delta t)} + U^{(-N\Delta t)}] \qquad (3.18)$$

and the process can then be repeated. To understand how this method works, consider the wave equation $\partial u/\partial t + c\partial u/\partial x = 0$, and suppose that initially u consists of a single "bump" of width If we apply Temperton's method once, with $T = N\Delta t$, assuming that we make no truncation error, we obtain

$$u^{(1)} = \tfrac{1}{2}[u^{(0)}(x - cT, 0) + u^{(0)}(x + cT, 0)].$$

If $cT \ll L$, $u^{(1)} \approx u^{(0)}$. If $cT \geq L$, $u^{(1)}$ will contain two bumps, with one half of the amplitude of the initial bump, and therefore the energy contained in u is now halved. This analysis suggests that T should be chosen in such a way that $c_s T \ll L_s$ for synoptic waves, and $c_g T \geq L_g$ for gravity waves. The optimum T found experimentally by Temperton, $T = 6\Delta t$, satisfies this criterion for the values of $c_g = 140$ m sec^{-1} and $L_g = 2\Delta y = 400$ km corresponding to his numerical model.

If we apply Temperton's method to a single harmonic component $U e^{i\omega t}$, with N = 6, we obtain a total damping

$$R_6 = 1 - 18p^2 + 48p^4 - 32p^6. \qquad (3.19)$$

This involves 12 computations of F and is also plotted on Fig. 3. Note that if Δt is taken as $1/\omega_m$, the maximum value allowable for stability, as done in Fig. 3, then the damping for low frequencies of Temperton's scheme is $R_6 \approx 1 - 18p^2$. The O-R scheme damping after 12 F computations is $R_{O-R} \approx 1 - 13.2p^2$. However, from Fig. 3 we see that Temperton's scheme does not provide damping at all frequencies unless the time step is taken as $\Delta t < 1/(2\omega_m)$. In that case Temperton's method becomes much less efficient than the O-R method even at low frequencies. It should also be noted that for odd N, Temperton's scheme will amplify high frequencies.

In summary we have shown from a linear analysis that of the six methods compared, the Okamura-Rivas scheme with n = 1, 1.6, 4, which is not necessarily optimum, provides the most efficient damping at low and middle frequencies, and the best damping at high frequencies.

Before closing the section we want to make two comments:

a) We have assumed that ω is a real number. This implies that irreversible terms, like friction, are not included, and amplifying or decaying modes, if present, need to have slow growth rates[2].

b) In this analysis we have not allowed for the restoration of heights after each iteration.

[2] Kálnay de Rivas (1975) has recently developed a simple scheme that will damp out <u>any</u> time dependent behaviour, and can be used, for example, to obtain an unstable steady state solution of the complete primitive equations, including forcing and dissipative terms.

4. Design of the numerical experiments

To test the various initialization techniques, a nonlinear, shallow-water model was developed, defined by the following equations:

$$\frac{\partial \phi u}{\partial t} = - \frac{\partial \phi uu}{\partial x} - \frac{\partial \phi uv}{\partial y} + f\phi v - \phi \frac{\partial \phi}{\partial x} \tag{4.1a}$$

$$\frac{\partial \phi v}{\partial t} = - \frac{\partial \phi uv}{\partial x} - \frac{\partial \phi vv}{\partial y} - f\phi u - \phi \frac{\partial \phi}{\partial y} \tag{4.1b}$$

$$\frac{\partial \phi}{\partial t} = - \frac{\partial \phi u}{\partial x} - \frac{\partial \phi v}{\partial y} \tag{4.1c}$$

where (u,v) are the horizontal velocity components, $\phi = gh$, and h is the height of the free surface. The Coriolis parameter is held constant, $f = 10^{-4} s^{-1}$.

In order to avoid nonlinear instability, an energy conserving finite difference scheme is used for the right hand side of (4.1). The grid used has $\Delta x = \Delta y = \Delta s = 250$ km.

In our experiments we artificially generate an initial state which is as closely in balance as possible. Then the velocity and height fields of the balanced data are altered or perturbed by various methods, and the different initialization techniques used to restore balance. We are interested in determining how well the initial "correct" fields are recovered, and how well in balance the initialized fields are.

The initial balanced state is generated by integrating the model for a finite time T with an artificial mass source term S(x,y,t) added to equation 4.1c. The integration is started from a state of rest with a level free surface at H = 3 km. A leapfrog marching procedure is used with a forward Euler step every 24 leapfrog steps to avoid the separation of fields at even and odd steps. The spatial variation of the source function is

$$S(x,y,t) = S(t) \sin\left(\frac{2\pi}{L} x\right) \sin\left(\frac{2\pi}{L} y\right)$$

where L = 4000 km. It is convenient to visualize the state produced as a checkerboard pattern extending periodically over the infinite f-plane. Numerical computations are made on a rectangular grid which extends one wavelength in the x direction and half a wavelength in the y direction. Boundary conditions are periodic, with the north-south boundaries matched diagonally to preserve periodicity.

We found that the degree of balance attained by the initial state was critically dependent on the time variation of the source term, S(t). The field shown in Fig. 4 is attained with the following form

$$S(t) = \frac{A\pi}{2T} \sin(\frac{\pi}{T} t)$$

where the integration was terminated at time T = 8 days, and A = 1.01 x $10^4 m^2 s^{-2}$. is the integrated strength. The contours are drawn at intervals of 60 m; the low is 340 m below the mean height, and the high 150 m above it. The associated velocity fields (not shown) are cyclonic around the low and anticyclonic around the high with 30 m s^{-1} maximum speed.

It was found necessary to add the source in very small increments (Δt = 5 min) in order to minimize the generation of imbalances in the initial state. After the source was "turned off", the forecast was continued using again the leap-frog scheme with Δt = 12 min. When the height at the point P (see Fig. 4) was monitored, it was found that the amplitude of inertial-gravity waves present was only 0.2 m, indicating a high degree of balance. Similar attempts to generate initial data were made using an exponential and a linear time dependence for S(t), with the same integrated strength. The resulting forecasts, after the source was turned off, showed gravity waves with amplitudes 25 and 100 times greater, respectively[3].

[3]This observation can have an important application in numerical climate studies, in which a physical parameter P (sea surface temperature, ground albedo, etc) is changed from its standard value P_0 to a different value P_1, to study the effect that this change has on the circulation. Our observations suggest that the initial imbalance, and consequently the amplitude of the transient inertia-

The initial fields (fig. 4) and the fields obtained after a 48 hours forecast are used as standards in computing rms departures of the velocity and height fields obtained using the initialization methods. In the initialization methods we allowed the option of restoring the geopotential heights after each iteration.

(cont) gravity waves generated by the change, are maximized by the common practice of changing P_0 to P_1 abruptly. On the other hand, a smooth change over a time T of the form

$$P(t) = \frac{P_0 + P_1}{2} + \frac{P_0 - P_1}{2} \cos \frac{\pi t}{T} , \quad 0 \leq t \leq T$$

will minimize the generation of gravity waves. When P is changed abruptly, P(t) is a Heaviside function, and its Fourier transform contains large amplitude high frequencies, which therefore excite gravity waves. When P is changed smoothly as we suggest, P and P' are continuous for $0 \leq t \leq T$, and if T is of the order of a few days, the transform of P(t) will contain only small amplitude high frequencies. We acknowledge a useful discussion with Mr. Mark Cane about this point.

5. Numerical results

As indicated in the previous section, a balanced "synoptic wave" with a geopotential amplitude of 250 m and maximum winds of 30 m s^{-1} was obtained and used as reference state for the initialization experiments.

In order to introduce initial imbalances representing the effect of observational errors, the reference fields were perturbed in two ways. First we assumed that the "observed" geopotential field contained no errors, but replaced the velocity field by the geostrophic velocity field. Second, we simulated observational errors by adding to the balanced fields normally distributed random numbers, with standard deviations typical of atmospheric measurement errors.

The damping of each iterative method was maximized by using the maximum time step (in whole minutes) for which the method remained stable. Table 2 compares these experimental values to the upper limit from the linear stability criteria as expressed in (3.12).

Note that the iterative schemes adhere to the linear criteria more closely than does the leapfrog scheme, and that for the NH2 method, there is strong damping of high frequencies even though $\omega_{max}\Delta t > 1$ (fig. 2).

a) Initialization of the geostrophically perturbed state

The geostrophically determined winds depart from the reference wind fields by an rms error of 7.7 m s^{-1}. If the forecast proceeds without initialization, gravity waves with amplitude of 125 m appear, which are sufficient to strongly distort the synoptic wave which has an amplitude of 250 m.

If the ellipticity condition (2.2) is satisfied everywhere, the balance equation can be solved without altering the geopotential field. Our reference state has enough amplitude that (2.2) is violated at a few points around the perimeter of the high. At the points where

$$x_{ij} = \frac{4(\bar{\phi}_{ij} - \phi_{ij})}{\Delta s^2} + \frac{f^2}{2} < 0, \qquad (5.1)$$

Method	Δt (nonlinear)	Δt (linear)
NH1	16 min	17 min
NH2	22 min	24 min
O	16 min	17 min
O-R	17 min	——
Leapfrog (forecast and Temperton's method)	12 min	17 min

Table 2: Maximum time steps according to the linear criteria and in the nonlinear numerical model.

we applied the following "correction". We defined $\phi'_{ij} = A\phi_{ij} + B\bar{\phi}_{ij}$, and from the conditions $A + B = 1$,

$$\frac{4(\bar{\phi}_{ij} - \phi'_{ij})}{\Delta s^2} + \frac{f^2}{2} = -\alpha x_{ij} ,$$

we determined A and B. Here, $\bar{\phi}_{ij}$ is the average geopotential at the four adjacent points, and α is a small non-negative number. After replacing ϕ_{ij} by ϕ'_{ij} at the points where $x_{ij} < 0$ we repeated the process until $x_{ij} \geq 0$ at all points. In our case, the best results were obtained with $\alpha = 0$, requiring 5 iterations. The height field was modified at 8 points, resulting in a maximum change of 0.5 m.[4]

Once the geopotential satisfied the ellipticity condition everywhere, 28 cycle-scan iterations were sufficient to solve the balance equation. Table 3 shows that the application of the balance equation reduces the rms wind error to 0.7 m sec^{-1}, and the amplitude of the residual gravity wave to 3m. We conclude that, in this case, the balance equation does provide a significant restoration of both the initial fields and their state of balance.

In additional experiments, however, we found that when the ellipticity condition was violated at a larger number of points the "correction" procedure became insufficient to "elliptize" the geopotential field. When the source strength was increased by 20% the correction procedure did not converge, and therefore we were unable to solve the balance equation. The iterative methods, of course, were not affected by the change in source strength. We will come back to this point in subsection 5c.

[4] An anonymous reviewer has pointed out the existence of a better "correction" procedure: Calculate $h = \nabla^2\phi + f^2/2$ at every point. Then solve for $\nabla^2\phi + f^2/2 = h^1$, where $h^1 = h$ if $h > 0$, $h^1 = \varepsilon$ if $h \leq 0$, and ε is a small positive number. ϕ^1 will satisfy the ellipticity condition.

In the first series of dynamic initialization experiments we performed 150 complete iterations with the NH1, NH2, 0 and O-R schemes, restoring the heights after each iteration. If we assume that each evaluation of the time derivative F (eq. 3.2) is equivalent to one timestep in a forward forecast, the equivalent time traversed in 150 iterations is 5 days for the NH1 method,

7.5 days for the NH2 method, and 2.5 days for the O and O-R methods.

Fig. 5a shows the decrease in rms error with the number of iterations. A considerable reduction of error occurs, but even 150 iterations are not sufficient for any method to converge to a steady value of the rms error. Figures 6a, b, c and d (lower curves) compare the forecasts of the height at the point P, when the heights are restored during initialization. Clearly, even 150 iterations are not sufficient to restore balance when the heights are not allowed to adjust freely. This can be understood in the following way: after the first iteration, the heights are modified from the original values with an rms change of 10-20 m, depending on the method. When we restore the geopotential field to correct this change, we are restoring a large portion of the initial imbalance. By restoring the heights after each iteration we force the slow convergence of the iterative methods.

In the next experiments we performed 150 iterations allowing the heights to adjust freely. Figures 5b and 5c show the variation of the rms wind and height errors with the number of iterations. Only the first 30 iterations are shown. All four methods reached a steady rms wind error of 6.9 m s^{-1} and created an rms height error of 46 m. To compare the convergence rates, we estimate the number of iterations required to reach the steady values: 40 (NH1), 15 (NH2), 15 (O) and 12 (O-R). The equivalent time traversed during these iterations is 32 h (NH1), 18 h (NH2), 6 h (O) and 5 h (O-R). Figures 6a, b, c and d (upper curves) show the height forecast at the point P when the heights adjusted freely during the 150 iterations. They show that high frequency oscillations with increasing amplitude appear in the forecasts after using NH1 and O. These are due to the aliasing of very high frequency waves not eliminated by the NH1 and O methods. On the other hand the NH2 and O-R methods completely eliminate these oscillations if the height is allowed to adjust. As shown in fig. 7, only 12 to 15 O-R iterations, or the equivalent of 5 to 6 hours of forecast, are enough to attain balance and eliminate inertia-

Method		rms error after initialization		rms error at the end of 48 hrs forecast		Amplitude of inertia-gravity wave during forecast
		height (m)	wind (m sec^{-1})	height (m)	wind (m sec^{-1})	
No perturbation		0	0	0	0	0.2
No initialization		0	7.7	29	8	150
Balance equation		0.1	0.7	1.5	1	3
NH1	heights restored 150 complete iterations	0	2.7	2.9	2.5	11
NH2		0	1.8	1.7	1.6	7
O		0	1.3	2.2	1.2	6
O-R		0	1.1	1.1	1.0	6
Temp. N=6		0	1.9	3.9	2.0	1
NH1	heights adjusted freely. 150 iterat.	46	6.9	129	10	0.2 → 10
NH2		46	6.9	46	6.7	0
O		46	6.9	617	76	1.4 → 200
O-R		46	6.9	46	6.7	0
Temp.	heights adj. 30 iterat.	44	6.8	48	6.8	2 → 15
"Best" Temperton		8.0	3.2	7.8	2.9	2
Gradient wind approx. (no initialization)		0	3.8	21.4	3.1	12
O-R with grad. wind		5.5	2.9	5.2	2.2	0

Table 3: Initialization of the geostrophically perturbed case

gravity waves from the forecast.

We made several experiments with Temperton's method. In the first we performed 150 complete iterations with N = 6, i.e. marched forward from the initial time $6\Delta t$, marched backward from the initial time $6\Delta t$, averaged the winds and restored the initial heights. Table 3 shows that the reduction of error is smaller than for the 0 and O-R methods, but there is more balance, as shown by the smaller amplitude of the residual inertia-gravity waves. It should be noted, however, that this method is 6 times more expensive in computer time than the O-R method. In fig. 5a the rms error is shown by the crosses plotted every 6 O-R iterations. Clearly the O-R method is much more efficient than Temperton's method.

When we allowed the heights to adjust freely during 30 Temperton iterations (equivalent to 180 O-R iterations), the rms errors were similar to those of the other schemes, but gravity waves with amplitudes of 2-15 m were present in the forecast; this agrees with our analysis in section 3, in that Temperton's scheme does not filter out high frequency waves uniformly.

As a last experiment, we tried Temperton's "best" scheme, in which heights were restored after each iteration during 10 iterations while velocities were allowed to adjust, followed by 10 iterations in which heights adjusted and winds were restored. We did obtain good results with this variation of Temperton's method, as shown by table 3. However this option still requires the equivalent of 120 O-R iterations, and fig. 7 shows clearly that in terms of balance, better results are obtained with just 12-15 O-R iterations.

No experiments have been made with Mesinger's scheme, but the linear analysis in section 3 indicates that the results would be qualitatively similar to those of the NH2 method.

b) Gradient wind approximation

The main effect of the approximation of the wind by its geostrophic value

is to overestimate the velocity field in the regions with cyclonic curvature and underestimate it in the anticyclonic regions. Therefore we can make a simple analysis of the adjustment problem for a geostrophic perturbation of the winds by assuming a perturbation of the form

$$\underset{\sim}{V}_o = \underset{\sim}{k} \times \nabla\psi_o \ , \quad \psi_o = \alpha \sin kx \sin ky, \quad \phi_o = 0.$$

From the linearized equation of conservation of potential vorticity we can obtain the perturbation geopotential ϕ_∞ that remains in geostrophic balance after inertia-gravity waves have been dissipated:

$$\nabla^2\psi_o - \frac{f}{\phi}\phi_o = \frac{1}{f}\nabla^2\phi_\infty - \frac{f}{\phi}\phi_\infty \ ,$$

from which

$$\phi_\infty = \beta \sin kx \sin ky, \quad \beta = \frac{\alpha f (kR_d)^2}{(kR_d)^2 + 1}$$

where $R_d = \frac{\sqrt{\phi}}{f}$ is the Rossby radius of deformation. Computing the energy $E = \iint (\phi \frac{V^2}{2} + \frac{\phi^2}{2})\, dx\, dy$, we obtain

$$E_\infty / E_o = (kR_d)^2 / ((kR_d)^2 + 1) \ .$$

This result indicates that in extratropical latitudes, where the scale of baroclinic waves is of the same order as the radius of deformation, most of the error introduced by the geostrophic estimation of the wind will remain present after adjustment. This is also apparent in our numerical experiments: when the heights were allowed to adjust, the reduction of rms wind error by the iterative schemes was small, while a significant modification of the observed height field was introduced (see TABLE 3). The main discrepancy occured near the low, where the geostrophic approximation strongly overestimated the winds and consequently the centrifugal force. During adjustment the height at the center of the low decreased from its original value of 2660 m to 2480 m, whereas

the center of the high increased from 3150 m to 3160 m.

We have seen that the common practice of restoring the mass fields after each iteration is not a solution to this problem, because it decreases enormously the efficiency of the dynamic initialization schemes. A better idea is to decrease the initial wind errors by the use of a more accurate approximation than the geostrophic for the initial winds. We found that a simple approximation of the gradient wind formula gave excellent results.

The gradient wind equation can be written as

$$V - V_g = \frac{V^2}{fr} \quad . \tag{5.2}$$

where V is the gradient wind, V_g the geostrophic wind and r the radius of curvature of the trajectory. The gradient wind approximation is strictly valid for circular steady flow but V approximates better than V_g the effects of flow curvature. However, the equation is quadratic in V and subject to a restriction, similar to the ellipticity condition, to ensure that the solution is real:

$$V_g + \frac{fr}{4} \geq 0. \tag{5.3}$$

If we assume that the right hand side of (5.2) is small compared to V_g, we can write $V = V_g(1 + \varepsilon)$ and neglect terms in ε^2. Then

$$\varepsilon \simeq - \frac{V_g}{fr + 2V_g} \quad . \tag{5.4}$$

The radius of curvature $R = - (1 + y')^{3/2}/y''$ can be estimated from the geostrophic streamlines: y' is the slope of a curve $\phi(x,y) =$ constant, and therefore $y' = - \phi_x/\phi_y$. Combining these formulas we obtain

$$r = - \frac{(\phi_x^2 + \phi_y^2)^{3/2}}{\phi_{xx}\,\phi_y^2 - 2\phi_x\phi_y\phi_{xy} + \phi_{xy}^2\phi_{yy}} \quad . \tag{5.5}$$

This formula allows the determination of r and V everywhere. In the regions where (5.3) is not satisfied, $|\varepsilon| > 0.5$, no longer a small number.

In these regions the correction of the geostrophic wind is not important because either V_g is small, and so is the error, or r is large, and therefore curvature effects are small. In our experiments we made no correction of the geostrophic wind whenever $|\varepsilon| \geq .5$.

This simple correction procedure was applied to the geostrophically perturbed state. The resulting rms wind error was 3.8 m s^{-1} compared to 7.7 m s^{-1} in the geostrophic error. When no further initialization was made, gravity waves had an amplitude of 12 m compared to 125 m in the geostrophic case. The O-R iterative scheme was applied allowing heights to adjust, and again it converged in about 12 iterations, eliminating gravity waves. Table 3 indicated that the rms height error after initialization was about 10 times smaller than in the geostrophically perturbed case[5]. However, these very encouraging results may be enhanced by the rather circular and steady state character of our basic flow (fig. 4).

c) Initialization of the randomly perturbed state.

In the previous experiments we have made no use of velocity measurements. In this section we describe a simulation of actual observations of both height and wind fields by perturbing the reference state fields with normally distributed random errors. The random errors are chosen to be compatible with real observational errors.

Three cases were run, with rms height errors of 0 m, 5 m and 10 m respectively. In all cases an error of 3 m s^{-1} rms was introduced on each component of the velocity field. In the three cases the gravity waves generated by the errors had an amplitude large enough to completely obliterate the reference forecast.

Only the iterative schemes NH2 and O-R were applied. The geopotential field was allowed to adjust and 150 complete iterations were performed. In both methods the rms error varied rapidly during the first 10 iterations and then attained

---

[5] Similar results have been reported by Gauntlett and Seaman (1974).

a quasi-steady value which continued to decrease very slowly as the iterations proceeded. Again gravity waves were completely eliminated by both methods. Table 4 presents the results and again we find that for the same number of complete iterations O-R is somewhat faster than NH2, even though one NH2 iteration requires 3 times more computations than one O-R iteration.

Another observation is that the magnitude of the height errors has no effect on the results. Again, this is explained by geostrophic adjustment analysis. Impulsive perturbations on the height with a spacial scale L will generate gravity waves which in an infinite domain move away to infinity, and in our experiments are dissipated by the iterative schemes. The remaining geostrophic mode contains most of the energy of the perturbation if $L >> R_d = \sqrt{\Phi}/f$, and very little energy if $L << R_d$ (see for example Charney, 1973). In the case of observational errors their scale is the grid size, much smaller than the radius of deformation, and therefore most of the height perturbations goes into the dissipated gravity waves. The opposite situation occurs with velocity perturbations, and, as shown in table 4, a large part of the energy of wind errors remain in the fields after balance has been attained. In any case, the size of errors after initialization is reasonably small, 6 m for the heights and 2 m s^{-1} for the wind speed.

With the balance equation approach only the heights were used. Case I, with no height errors, coincides with the case discussed in section 5a. In case II, we were able to "correct" the heights as described in section 5a, and satisfy the ellipticity condition everywhere, but the cycle-scan method of solution of the balance equation failed to converge. In case III the ellipticity condition was violated at many points and the "correction" procedure failed to determine an elliptic geopotential field. Therefore we were unable to solve the balance equation in cases II and III.

The ellipticity condition (5.1) can be written as

	rms error		Method	rms error after initialization		amplitude of gravity wave during 48 h forecast
	height (m)	wind ($m\ sec^{-1}$)		height (m)	wind ($m\ sec^{-1}$)	
Case I	0	4.2	None	—	—	40-350
			NH2	6.4	2.0	0
			O-R	6.2	2.0	0
			Balance	0.1	0.7	3
Case II	5	4.2	None	—	—	120-350
			NH2	6.5	1.9	0
			O-R	6.3	1.8	0
			Balance	No convergence		
Case III	10	4.2	None	—	—	70-350
			NH2	6.6	1.9	0
			O-R	6.5	1.8	0
			Balance	"Correction" procedure failed		

Table 4. Random perturbations on the reference state.

$$\Delta h = h - \bar{h} < \frac{f^2 \Delta s^2}{8g} \tag{5.6}$$

In this form, it is a restriction on the difference between the height at a point and the average height at the 4 adjacent points. It becomes increasingly stringent as the model resolution is increased. For example, with Δs = 250 km and $f = 10^{-4} sec^{-1}$, Δh_{max} = 8 m, but if Δs = 125 km, the ellipticity condition is violated when Δh > 2 m! This is a serious drawback of the balance equation approach, especially since the tendency of modern NWP models is towards smaller grid sizes.

6. Summary and conclusions

We have presented a linear analysis and comparison of the damping properties of six initialization schemes: the two proposed originally by Nitta and Hovermale (1969), the one by Mesinger (1972), a scheme attributed to Okamura (Nitta, 1969, Appendix), Temperton's (1973) averaging scheme and a modification of Okamura's scheme by Kálnay de Rivas. The linear analysis indicates that the Okamura-Rivas scheme has the most efficient damping properties over the whole frequency range, suggesting that it should be faster than the other methods and give more stable results.

A nonlinear shallow water equations model on an f-plane has been used to test the initialization schemes and the results agree well with the linear analysis. When the heights are recovered after each iteration, the iterative methods have a very slow convergence rate, because most of the imbalance is also recovered after each iteration. When the heights are allowed to adjust freely, the iterative schemes converge much faster. In particular, the Okamura-Rivas scheme attains complete balance in only 12-15 iterations, equivalent to about 5 to 6 hours of regular forecasting using the leapfrog scheme.

In the case of a geostrophic perturbation of the reference state, in which the observed winds are replaced by their geostrophic values, most of the error energy remains in the fields after free adjustment. This is in agreement with linear adjustment theory since the perturbation occurs in scales similar to the radius of deformation.

Observational errors are also simulated by the introduction of random errors into the reference heights and velocity fields. In this case the dynamic initialization methods converge to a state much closer to the reference state than in the case of a geostrophic perturbation. In accordance with adjustment theory, small scale height errors are dissipated into gravity waves, while a significant portion of the small scale velocity error energy is retained in the

final fields.

We conclude that whenever available, reliable wind observations should be included in the initial data for the dynamic initialization methods. The smoothing incorporated in conventional analysis techniques may also help to reduce the errors in the observed fields. In data-sparse regions we suggest the use of a simple gradient wind approximation which can be directly evaluated from the geopotential field. In our experiments this approximation produced much better results than the geostrophic wind approximation. Another method to improve the initial estimation of the wind field can be to solve the balance equation on a coarse grid in data-sparse regions and then interpolate to finer resolution. In any case the best procedure is to first obtain a good estimate of the initial fields and then apply the iterative technique, allowing the free adjustment of the mass field.

The balance equation approach provides good but not complete balance in the initial state for a primitive equation model. However this approach depends very critically on the ellipticity condition, which in its simplest form is a restriction on the maximum amount by which the height at a point can exceed the average height at the neighboring points. We have reported that this restriction is severely violated around strong anticyclones and, when the resolution is increased, by measurement errors typical of those occurring in atmospheric observations. The ellipticity condition does not affect the iterative techniques. When free adjustment is allowed the dynamic initialization methods become not only simpler but faster than the balance equation approach. In our numerical model, the Okamura-Rivas scheme required for convergence at least an order of magnitude less computations than the balance equation method.

We have made our tests in a simple shallow water equations model, with high frequency inertia-gravity waves. In baroclinic primitive equations models, inertia-gravity waves can have frequencies with values as low as the Coriolis

parameter. It is in these models that the flexibility of the Okamura-Rivas method may be put to maximum use. Even with the sequence n = 1, 1.6, 4, which is not optimum, and a time step of 15 minutes, waves with a frequency $\omega = f = 10^{-4} s^{-1}$ will be reduced by 20% in 12 Okamura-Rivas iterations, and only by 4% using the Nitta-Hovermale schemes and the same number of computations.

The problem of four-dimensional data assimilation has not been considered here, but our results suggest that the use of the Okamura-Rivas scheme may be extremely useful in damping gravity waves generated by the introduction of new data in a model. A few Okamura-Rivas iterations after each set of data is introduced followed, if necessary, by the use of a dissipative time scheme, will probably be sufficient to ensure a successful assimilation.

References

Bolin, B., 1955: Numerical forecasting with the barotropic model. Tellus, 7, 27-49.

Charney, J.G., 1955: The use of primitive equations of motion in numerical prediction. Tellus, 7, 22-26.

Charney, J.G., 1973: Planetary fluid dynamics. Dynamic Meteorology, P. Morel, editor, D. Reidel Publishing Company, Dordrecht, Holland, 97-351.

Gauntlett, D.J. and R.S. Seaman, 1974: Four - dimensional data assimilation experiments in the Southern Hemisphere. J.Atmos. Sci., 13, 845-853.

Houghton, D. and W.M. Washington, 1969: On global initialization of the primitive equations: Part I. J. Appl. Meteor., 8, 726-737.

Houghton,D., D.P. Baumhefner and W. M. Washington, 1971: On global initialization of the primitive equations: Part II. J. Appl. Meteor. 10, 626-634.

Kalnay de Rivas, E., 1975: A numerical scheme for the solution of unstable boundary value problems. (in preparation).

Mesinger, F., 1972: Computation of the wind by forced adjustment to the height. J. Appl. Meteor., 11, 60-71.

Miyakoda, K., 1956: On a method of solving the balance equation. J. Met Soc. Japan, 24, 364-367.

Miyakoda, K., 1960: Numerical solution of the balance equation. Tech Rep. Japan Meteor. Agency, No. 3, 15-34.

Nitta, T., 1969: Initialization and analysis for the primitive equation model. Proceedings of the International WMO/IUGG Symposium on Num. Wea. Pred. in Tokyo, 1968, The Meteor. Soc. of Japan, pp VI-11 to VI-20.

Nitta, T. and J.B. Hovermale, 1969: A technique of objective analysis and initialization for the primitive forecast equations. Mon. Wea. Rev., 97, 652-658.

Petterssen, S., 1953: On the relation between vorticity, deformation, and divergence and the configuration of the pressure field. Tellus, 5, 231-238.

Phillips, N.A., 1960: On the problem of initial data for the primitive equations. Tellus, 12, 121-126.

Richardson, L.F., 1922: Weather Prediction by Numerical Process. London: Cambridge University Press, 236 pp.

Shuman, F.J., 1957: Numerical methods in weather prediction: I: The balance equation. Mon. Wea. Rev., 85, 329-332.

Temperton, C., 1973: Some experiments in dynamic initialization for a simple primitive equation model. Quart. J. Roy. Meteor. Soc., 99, 303-319.

Winninghoff, F.J., 1973: Not on a simple restorative-iterative procedure for initialization of a global forecast model. Mon. Wea. Rev., 101, 79-84.

Figure Captions

Figure 1: Reduction of amplitude after one complete iteration for the NH1, NH2, and O-R scheme.

Figure 2: Comparison of the relative efficiency of the NH1, NH2, O and O-R iterative schemes. Reduction of amplitude after 12 F computations.

Figure 3: Same as Fig. 2 except for the Temperton, Mesinger and Okamura-Rivas schemes.

Figure 4: Reference height field. P indicates the point at which the height was monitored during the forecast.

Figure 5: Reduction of error during initialization. a) rms velocity error when the geopotential is restored after each iteration. b) rms velocity error during free adjustment. c) rms height error during free adjustment.

Figure 6: Height forecast at the point P. Lower curves: heights restored after each iteration. Upper curves: heights adjusted freely. The reference forecast is also indicated. The initialization scheme used was a) Nitta-Hovermale 1, b) Nitta-Hovermale 2, c) Okamura, d) Okamura-Rivas.

Figure 7: Comparison of the height forecast at point P obtained after 12 and 15 Okamura-Rivas iterations and after 20 "best" Temperton iterations.

Acknowledgements

We are very grateful to Prof. N.A. Phillips who contributed to the early planning of the experimental technique, and to Profs. J.G. Charney and E.N. Lorenz for some useful discussions. The computations were performed at the National Aeronautics and Space Administration (NASA) Goddard Institute for Space Studies in New York (NASA Grant NGR 22-009-727). This work was supported by the National Science Foundation under Grant no. NSF OCD71-00333. W. K-F Grant acknowledges support from the Air Force Institute of Technology (U.S. Air Force).

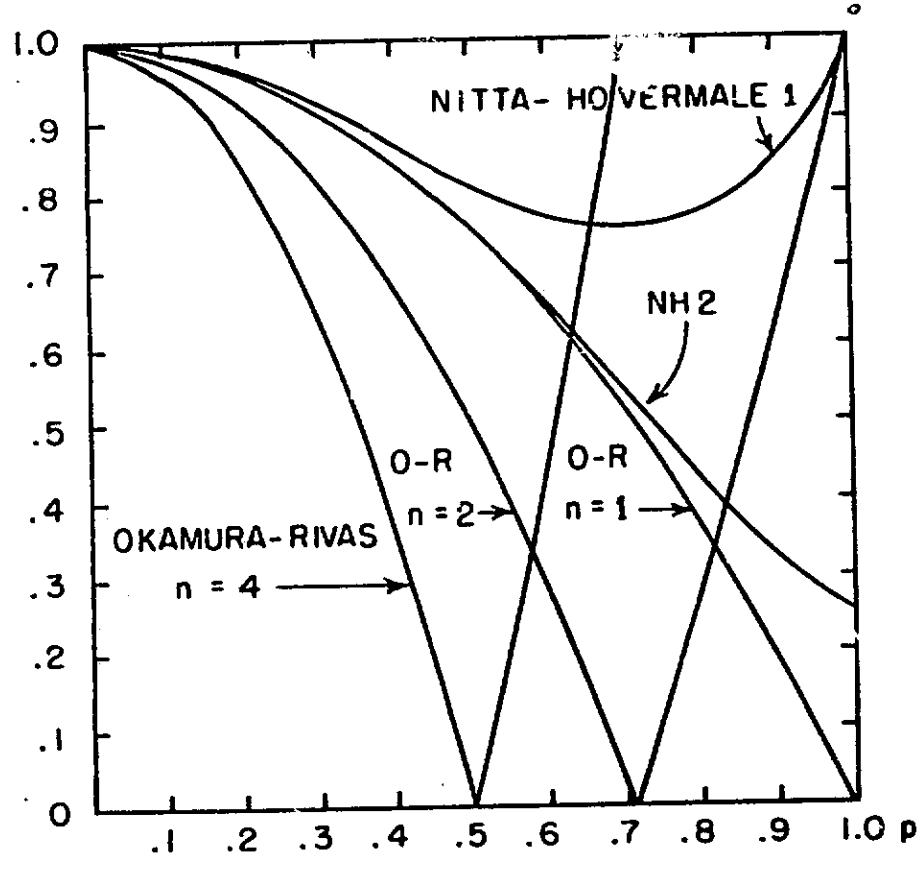

Fig 1

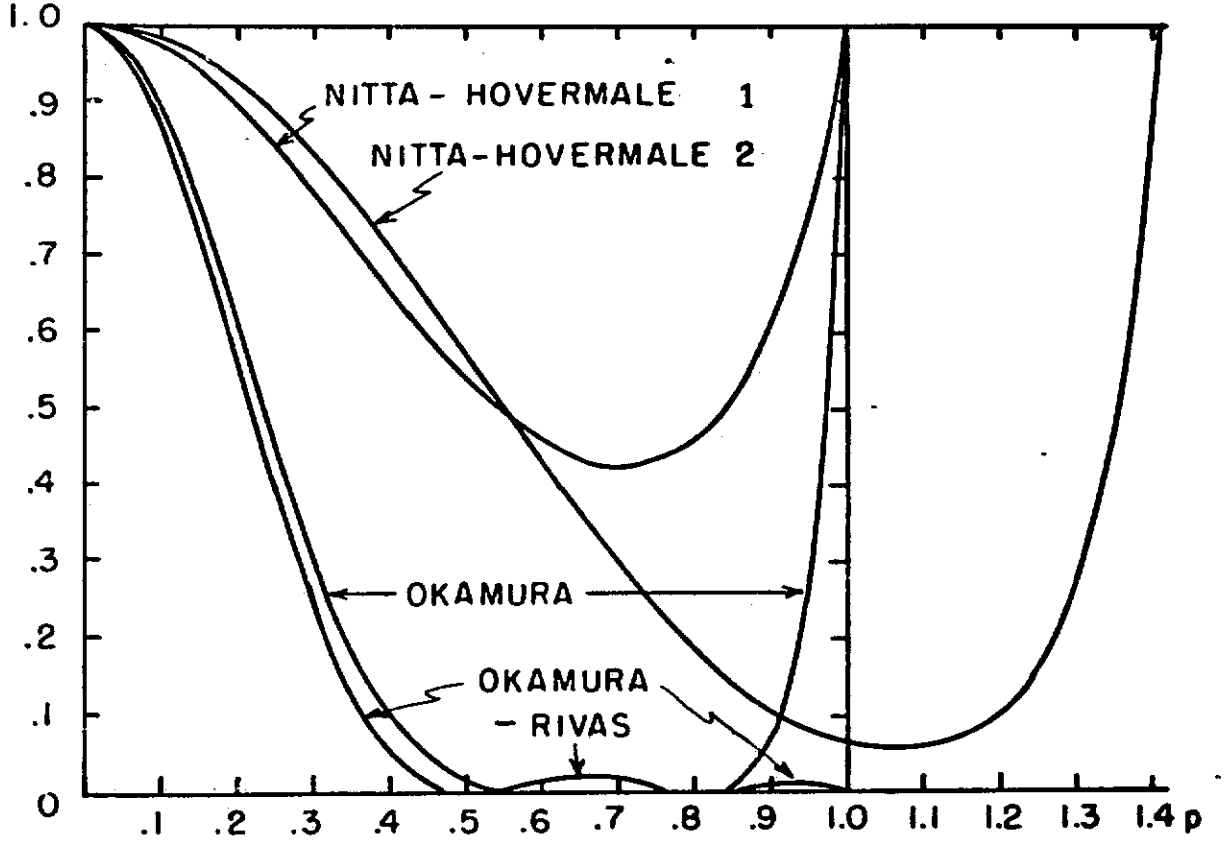
1.0
.9
.8
.7
.6
.5
.4
.3
.2
.1
0
NITTA - HOVERMALE 1
NITTA-HOVERMALE 2
OKAMURA
OKAMURA
- RIVAS
.1
.2
.3
.4
.5
.6
.7
.8
.9
1.0
1.1
1.2
1.3
1.4 p

Fig 2

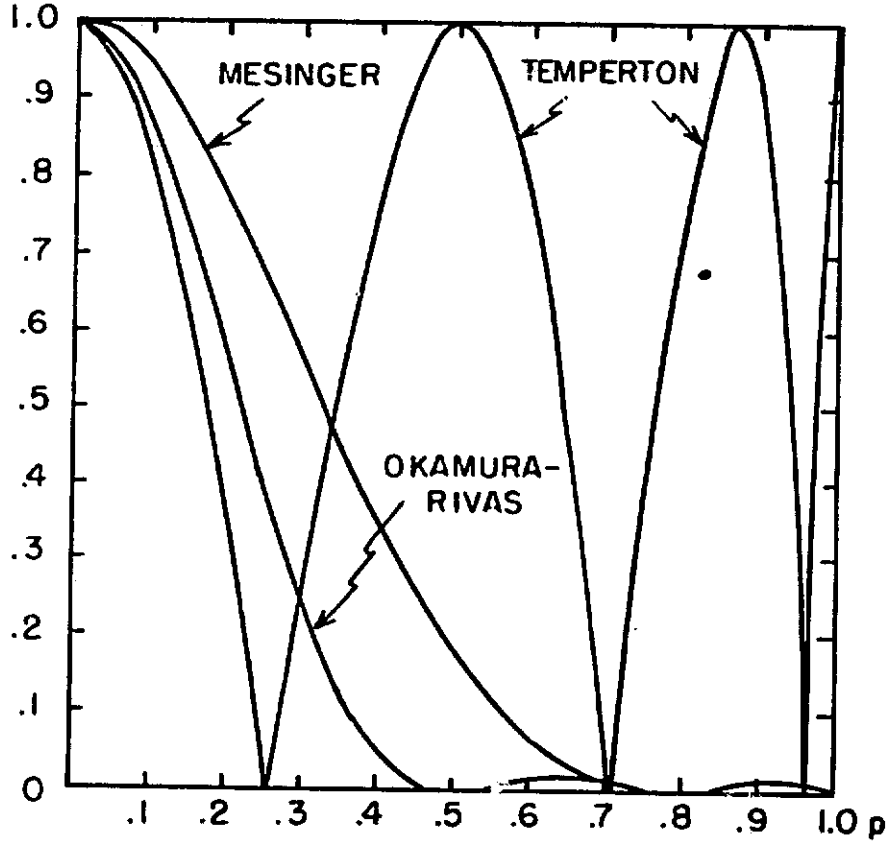
1.0
.9
.8
.7
.6
.5
.4
.3
.2
.1
0
MESINGER
TEMPERTON
OKAMURA-
RIVAS
.1
.2
.3
.4
.5
.6
.7
.8
.9
1.0 p

Fig 3

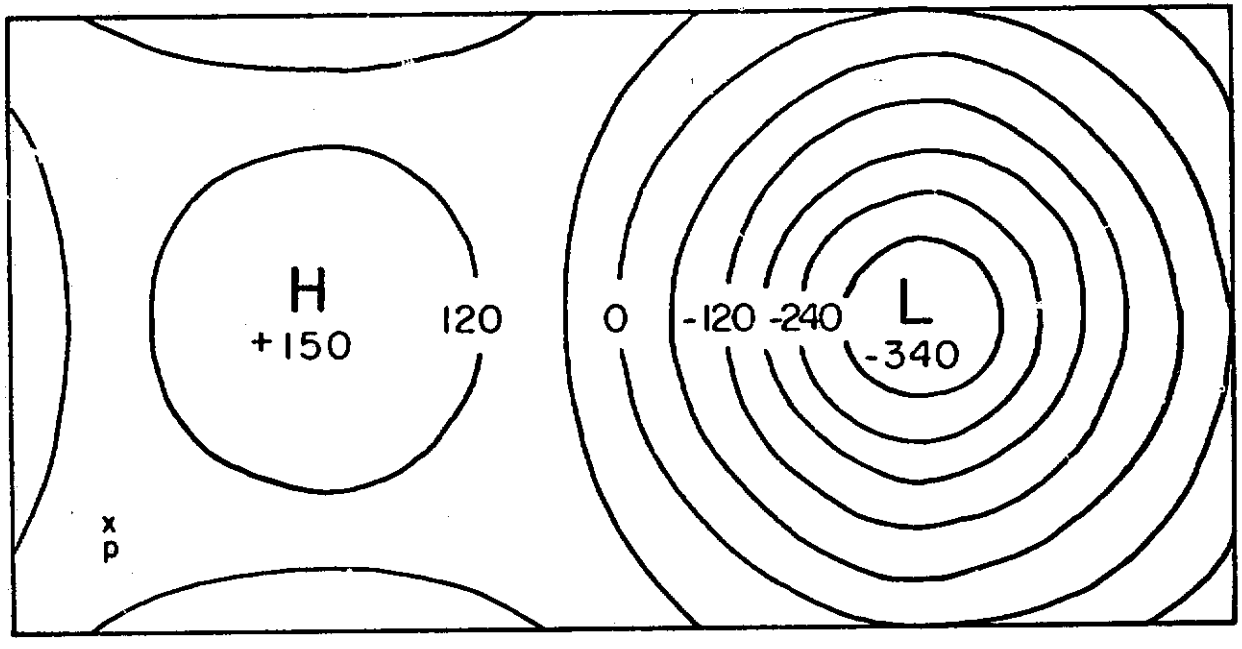

Fig 11

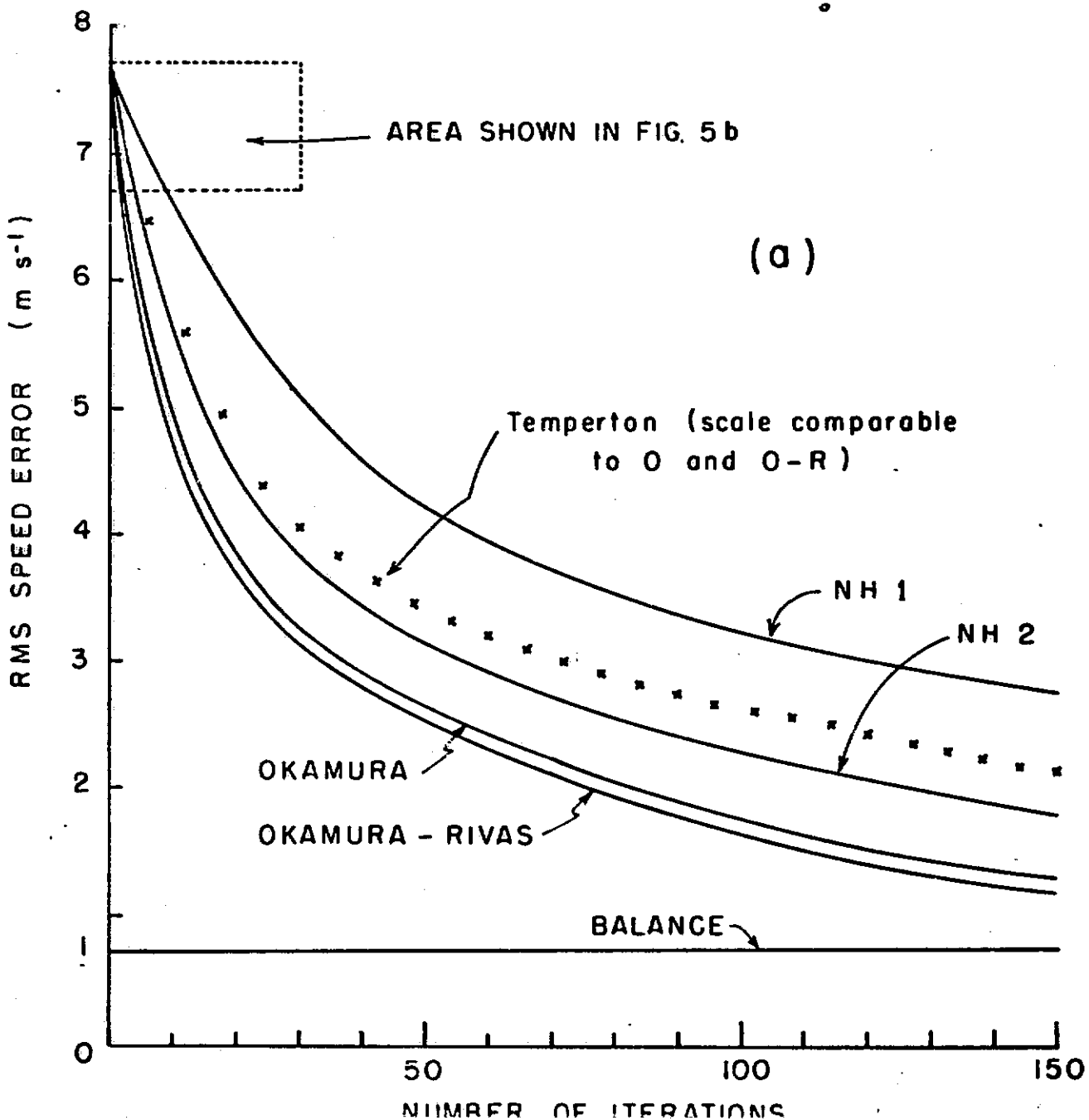
AREA SHOWN IN FIG. 5b
(a)
Temperton (scale comparable to O and O-R)
NH 1
NH 2
OKAMURA
OKAMURA - RIVAS
BALANCE
RMS SPEED ERROR (m s⁻¹)
NUMBER OF ITERATIONS
0
1
2
3
4
5
6
7
8
50
100
150

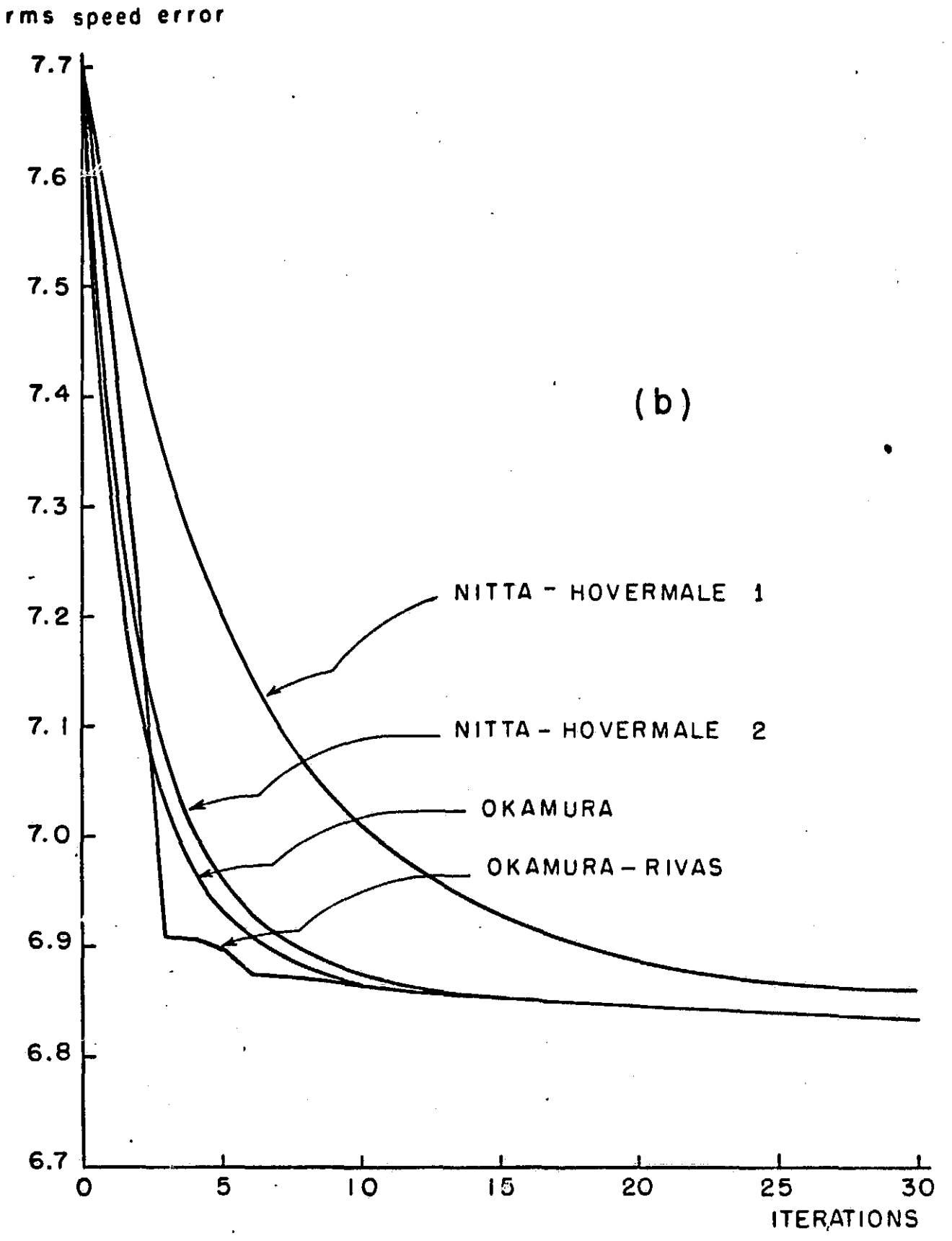
rms speed error
7.7
7.6
7.5
7.4
7.3
7.2
7.1
7.0
6.9
6.8
6.7
0
5
10
15
20
25
30
ITERATIONS
(b)
NITTA - HOVERMALE 1
NITTA - HOVERMALE 2
OKAMURA
OKAMURA – RIVAS

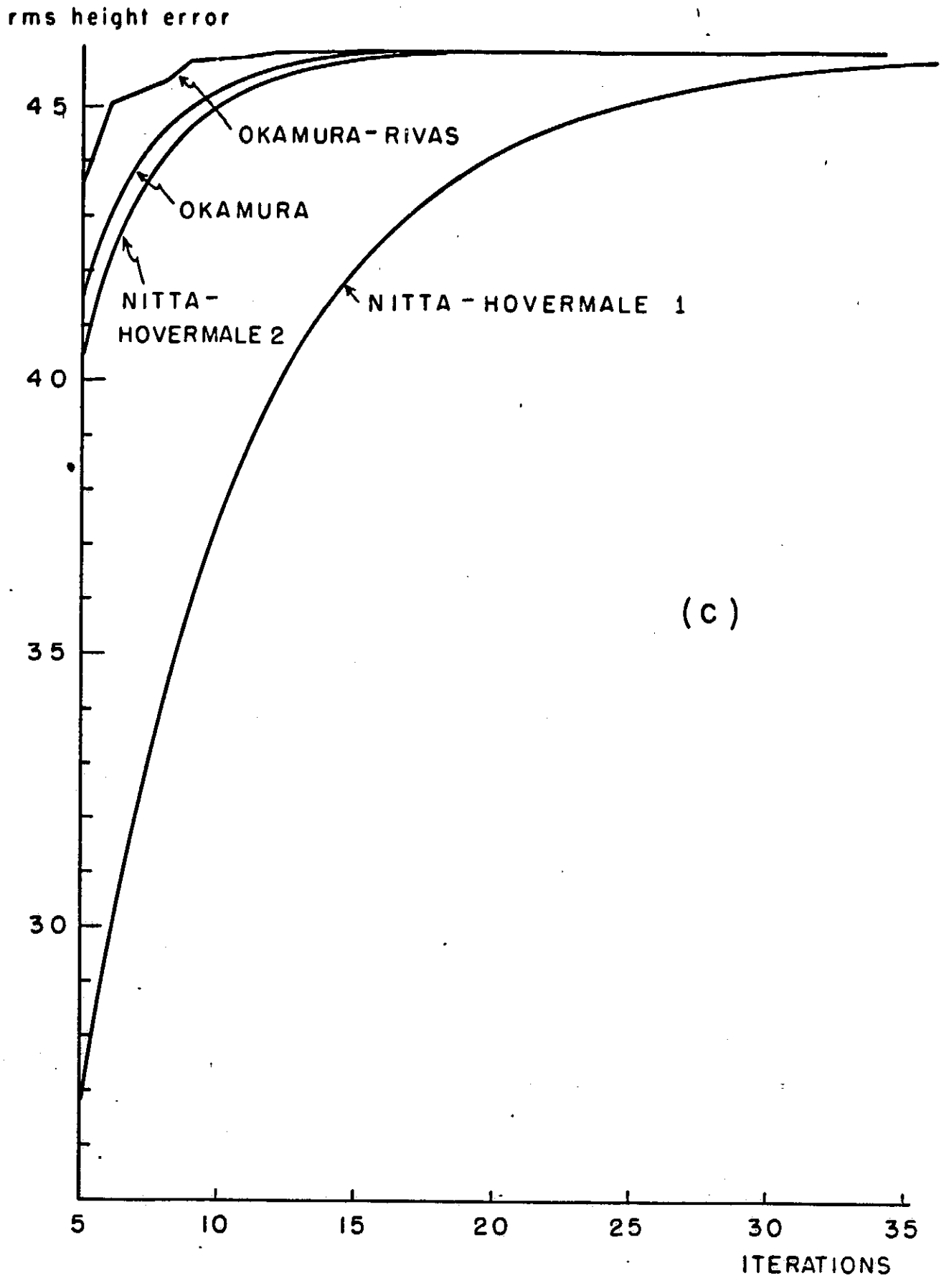
rms height error
45
40
35
30
OKAMURA-RIVAS
OKAMURA
NITTA-
HOVERMALE 2
NITTA-HOVERMALE 1
(C)
5
10
15
20
25
30
35
ITERATIONS

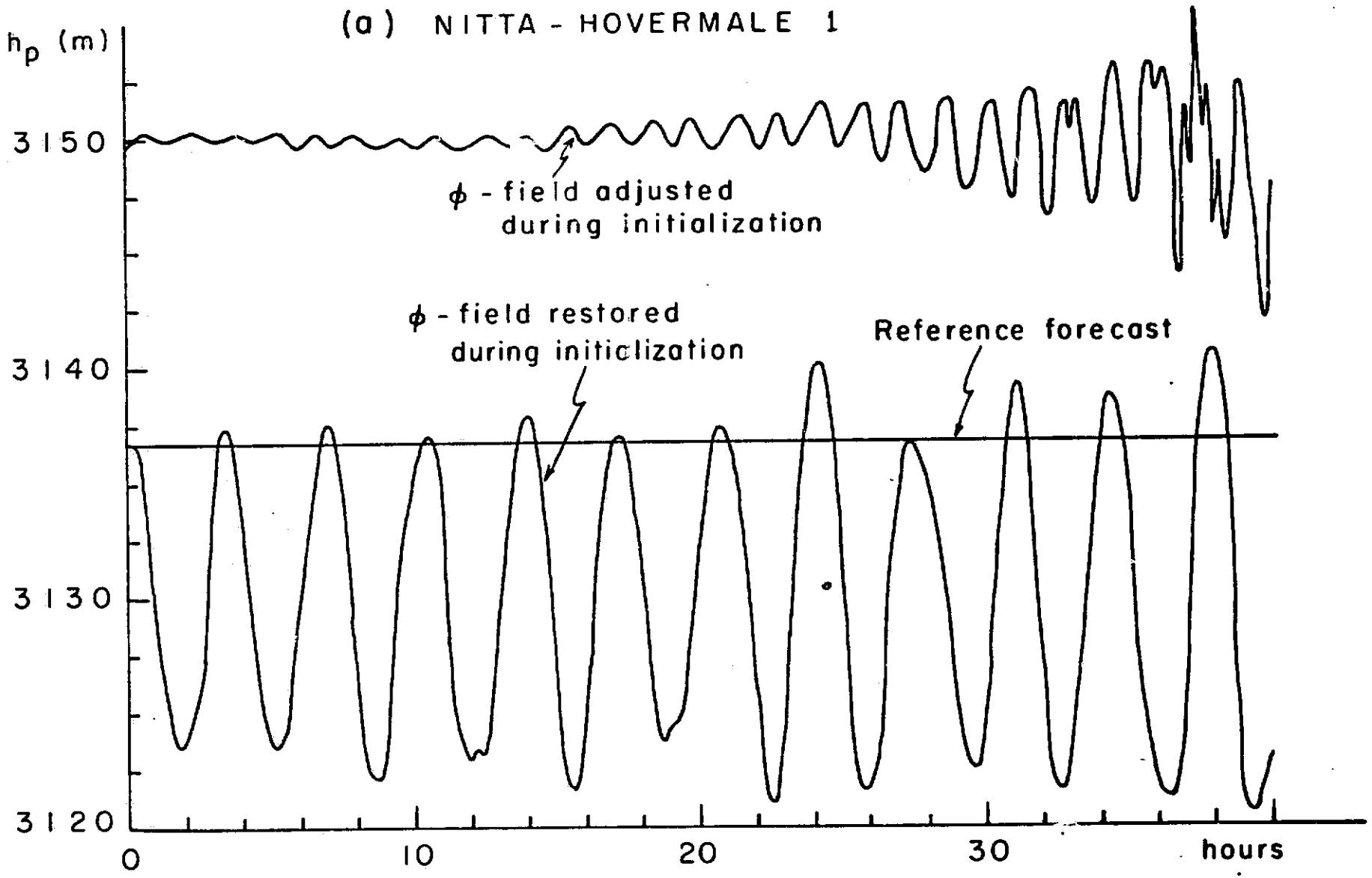
(a) NITTA - HOVERMALE 1
h_p (m)
3150
3140
3130
3120
0
10
20
30
hours
ϕ - field adjusted during initialization
ϕ - field restored during initiclization
Reference forecast

(b) NITTA - HOVERMALE 2

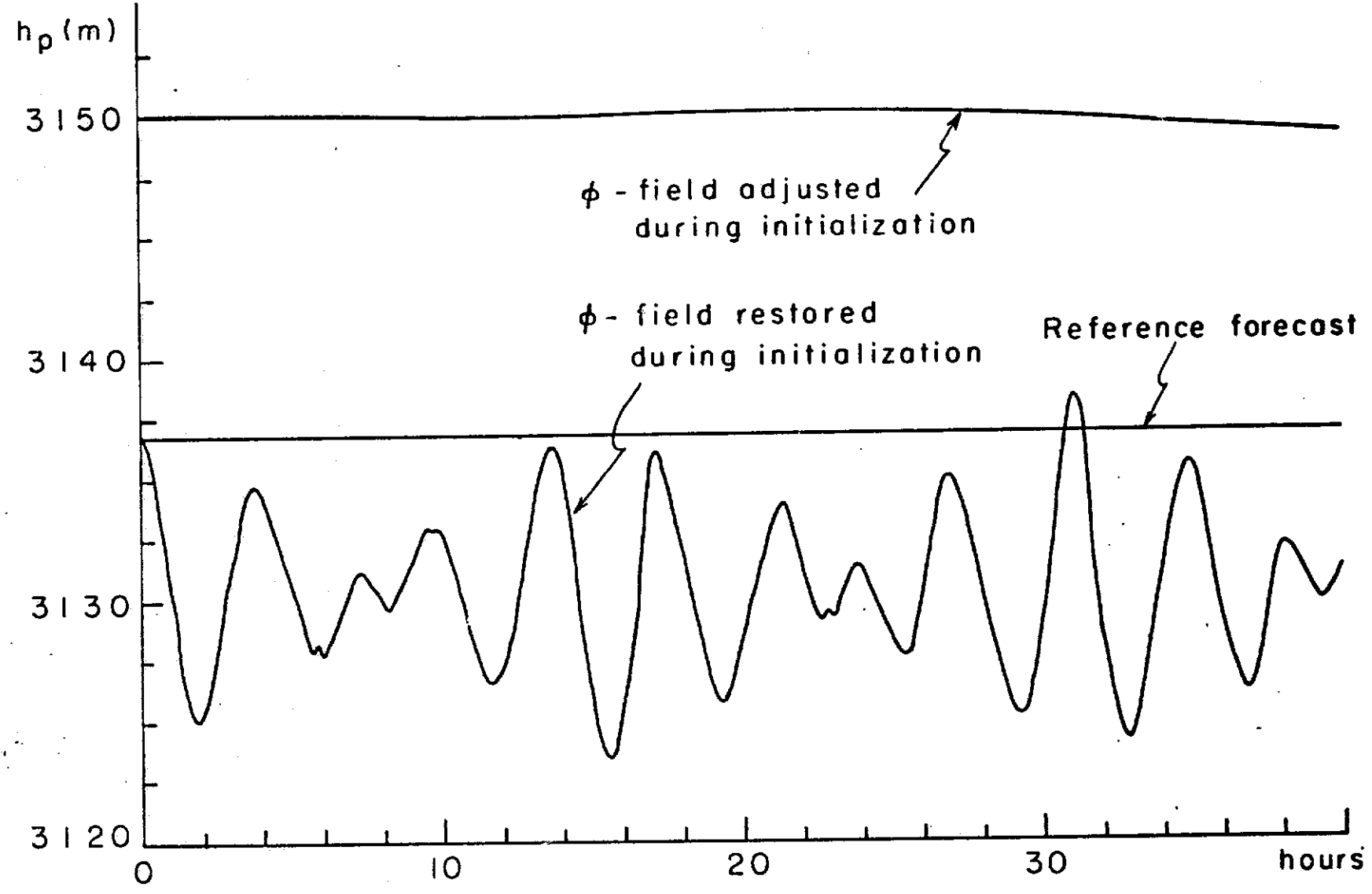

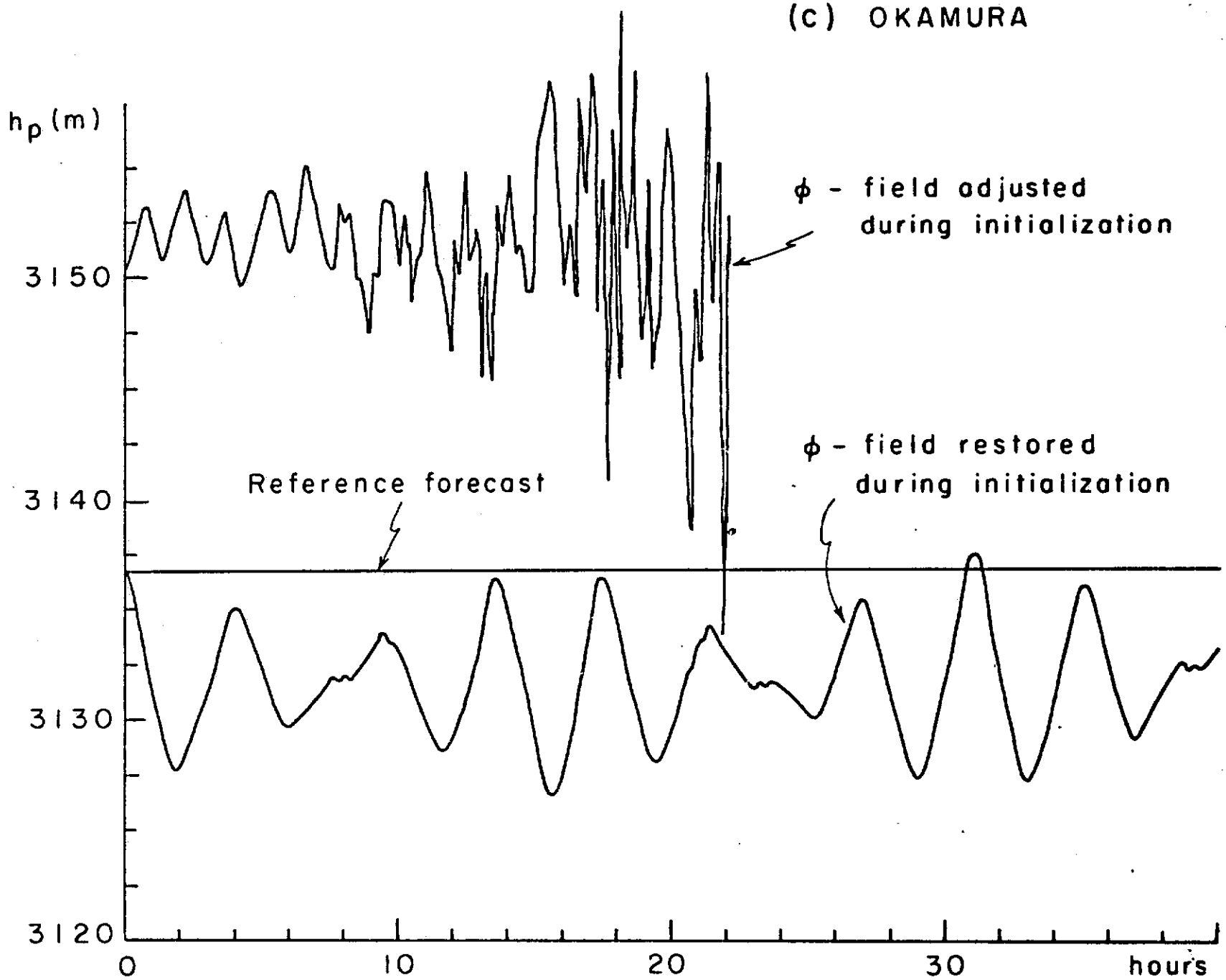
(c) OKAMURA
h_p (m)
3150
3140
3130
3120
0
10
20
30
hours
ϕ - field adjusted during initialization
ϕ - field restored during initialization
Reference forecast